Journal of Science and Technology in Civil Engineering, HUCE, 2026, 20 (2): 20–32

CFD MODELING OF MUDFLOW IMPACT ON RIGID BARRIERS USING THE HERSCHEL–BULKLEY RHEOLOGY

Nhu H. T. Nguyen[a], Thanh-Trung Vo[b], Tran-Hieu Nguyen[c], Ngoc-Phan Nguyen[d], Trung-Kien Nguyen[c,*]

[a]*Faculty of Science Engineering and Built Environment, School of Engineering, Deakin University, Geelong Waurn Ponds Campus, 75 Pigdons Road, Waurn Ponds, Victoria 3216, Australia*
[b]*School of Transportation Engineering, Office of Research Administration, Danang Architecture University, 566 Nui Thanh road, Hai Chau ward, Danang city, Vietnam*
[c]*Faculty of Building and Industrial Construction, Hanoi University of Civil Engineering, 55 Giai Phong road, Bach Mai ward, Hanoi, Vietnam*
[d]*CPT Group Joint Stock Company, Heritage West Lake Building, 677 Lac Long Quan Street, Tay Ho ward, Hanoi, Vietnam*

Article history:
Received 05/11/2025, Revised 31/12/2025, Accepted 11/02/2026

Abstract

This study employs a Computational Fluid Dynamics (CFD) approach to simulate the dynamics of non-Newtonian mud/debris flows impacting rigid barriers under flume-scale conditions. The flow is modeled using the Herschel–Bulkley rheology to capture both yield stress and shear-thinning behavior characteristics of mud materials. Numerical simulations are performed with OpenFOAM for 12 configurations varying in slope inclination (0°–15°) and barrier position relative to the slope toe. The model is first validated against experimental data, showing good agreement in terms of pressure evolution and velocity profiles. The numerical results reveal that flow behavior is strongly governed by the interplay between gravitational acceleration, yield stress effects, and energy dissipation within the basal shear layer. Increasing the slope angle enhances the conversion of potential to kinetic energy, leading to higher impact velocities, larger runup heights, and greater impact forces. Conversely, increasing the distance between the slope toe and the barrier promotes viscous dissipation, thereby reducing the available impact energy. Notably, for the steepest slope (15°), the effect of barrier distance becomes minor due to compensation between acceleration and front spreading. These findings provide new insights into energy conversion mechanisms and their implications for the design and placement of protective barriers in mud/debris flow prone areas.

Keywords: mudflow; debris flow; CFD; non-Newtonian fluid; Herschel–Bulkley model.

https://doi.org/10.31814/stce.huce2026-20(2)-02

1. Introduction

Mud and debris flows are among the most destructive mass-movement processes in mountainous regions, posing severe risks to infrastructure and human life. These flows, consisting of mixtures of water, fine sediment, and coarse particles, exhibit non-Newtonian behavior characterized by yield stress and shear-thinning viscosity [1, 2]. The rapid downslope motion and sudden impact against protective structures make the prediction of mobility, impact force, and runup height a critical topic in hydraulic and geotechnical engineering [3–6].

In particular, mud and debris flow mixtures possess distinctive rheological characteristics, including a finite yield stress below which the mixture behaves as a plug layer, and a shear-dependent (typically shear-thinning) viscosity that governs deformation once the yield stress is exceeded. After

*Corresponding author. *E-mail address:* kiennt3@huce.edu.vn (Nguyen, T.-K.)

yielding, the material flows as a viscoplastic fluid whose resistance is controlled by both the fine-grained matrix and interactions among coarse grains. These rheological features strongly influence front propagation, internal shear structure, runout behavior, and impact forces, thereby necessitating constitutive models capable of representing viscoplastic behavior.

Physical modeling studies provided valuable insight into front kinematics, deposition patterns, and impact pressures, but were limited by difficulties in capturing internal flow structure and temporal evolution of flow energy [7, 8]. Advances in computational methods such as computational fluid dynamics (CFD) and smoothed particle hydromechanics (SPH) methods have enabled detailed simulation of debris and mud flows with complex rheological behavior [9–11]. The rheological complexity of debris and mud flows requires constitutive models to be capable of capturing both the yield stress and shear-dependent viscosity. Among others, the Herschel–Bulkley model has been widely adopted in both experimental and numerical analyses to describe such viscoplastic flow behavior [2, 12]. Using this model, several CFD and SPH studies have successfully reproduced dam-break experiments and real debris flow surges, thereby validating flow velocity, depth, and impact pressure against laboratory measurements [10, 13].

Recent research has highlighted the influence of slope geometry and barrier configuration on the dynamics of debris flow impacts. Increasing slope inclination enhances the downslope component of gravity and therefore increases the conversion rate of potential to kinetic energy, while longer travel distances before impact allow greater dissipation through spreading and frictional losses [14, 15]. However, despite numerous physical and numerical studies focusing on runup height and impact force [16–19], the systematic connection between flow energy and transformation, slope inclination, and barrier distance has not been sufficiently explored for non-Newtonian flows.

This study aims to fill that gap through a series of numerical simulations using the Volume of Fluid (VOF) method with Herschel–Bulkley model implemented in OpenFOAM. VOF is an extension of CFD to simulate multiphase fluid flows with immiscible interfaces, making it particularly suitable for simulating debris/mud flows, which involve free-surface flows exposed to air. The model reproduces flume-scale dam-break type mudflow experiments with varying slope angles (0°, 5°, 10°, 15°) and barrier distances from the toe of slope. The paper (i) quantifies the temporal evolution of potential, kinetic, and dissipated energies; (ii) determines runup height and impact force; and (iii) interprets the results within an energy-based framework. The findings contribute to a better understanding of how slope-driven acceleration and pre-impact dissipation jointly determine impact severity, providing implication for the design and placement of protective barriers in debris-flow-prone areas.

2. Methodology

In this section, we briefly introduce the governing equations of VOF method. This is followed by a concise comparison of several rheological models, with an emphasis on the Herschel–Bulkley model.

2.1. Brief introduction of the VOF method

Similar to CFD, VOF is a Eulerian-based method in which the computational domain is discretized into a finite number of control volumes (cells). The governing equations, including the conservation of mass and Navier–Stokes equations, are then solved over this discretized domain [20–22].

The conservation of mass equations ensures continuity in the flow. For incompressible flow, it remains the same as in the standard CFD formulation:

$$\nabla \cdot \mathbf{u} = 0 \tag{1}$$

where $\mathbf{u}$ denotes the velocity vector.

The Navier–Stokes equations for a two-phase flow in the VOF framework are expressed as:

$$\frac{\partial(\rho\mathbf{u})}{\partial t} + \nabla\cdot(\rho\mathbf{u}\otimes\mathbf{u}) = -\nabla p + \nabla\cdot\left(\mu\left(\nabla\mathbf{u} + \nabla^T\mathbf{u}\right)\right) + \rho\mathbf{g} + \mathbf{F}_\sigma \tag{2}$$

where p is the pressure, ρ is the local density, μ is the dynamic viscosity, p is the pressure, $\mathbf{g}$ is the gravitational acceleration vector and $\mathbf{F}_\sigma$ represents the surface tension force.

The local properties ρ and μ are computed as weighted averages based on the volume fraction α:

$$\begin{aligned}\rho &= \alpha\rho_1 + (1-\alpha)\rho_2\\ \mu &= \alpha\mu_1 + (1-\alpha)\mu_2\end{aligned} \tag{3}$$

where ρ_1, μ_1 and ρ_2, μ_2 are the density and viscosity of first and second fluid phase, corresponding to mud flow and air in this study. α is the first phase volume fraction which is obtained by solving the transport equation:

$$\frac{\partial\alpha}{\partial t} + \mathbf{u}\cdot\nabla\alpha = 0 \tag{4}$$

2.2. Herschel–Bulkley rheological model

Mudflows exhibit non-Newtonian behavior due to their complex composition, which includes water, fine sediments, and possibly coarse particles [2, 24]. As a result, their flow behavior is characterized by a yield stress and a shear-thinning viscosity that varies with the shear rate. The Newtonian model, which assumes a linear relationship between shear stress and shear rate and does not account for yield stress, fails to accurately capture the complex behavior of mudflows [25]. Therefore, more advanced rheological models are required to provide a more realistic representation of mudflow characteristics. A comparative illustration of commonly used rheological models for simulating flow mobility is presented in Fig. 1.

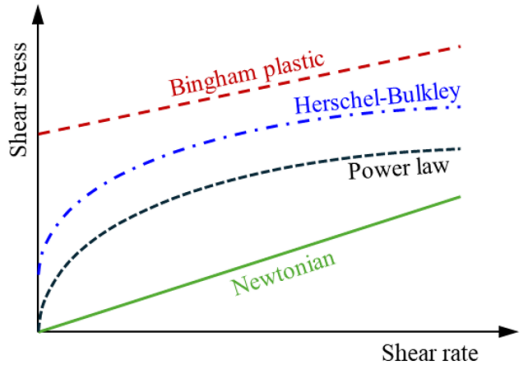

Figure 1. Comparison of different rheological models (modified after [23])

Among several advanced rheological models, the Herschel–Bulkley is widely recognized as suitable for describing the viscoplastic behavior of mud and debris flows in which the fluid exhibits either linear or non-linear viscous behavior depending on the shear stress condition.

The shear stress for incompressible fluids is described as:

$$\tau = \mu\left(\nabla\mathbf{u} + \nabla^T\mathbf{u}\right) \tag{5}$$

where μ is the fluid viscosity, which is formulated in the Herschel–Bulkley model implemented in OpenFOAM as follows:

$$\mu = \min\left(\mu_0, \tau_0/\dot{\gamma} + k\dot{\gamma}^{n-1}\right) \tag{6}$$

where τ and $\dot{\gamma}$ are shear stress and shear strain rate; τ_0 is the yield stress, k is the consistency index and n is the flow index. For low strain rates, the material is modelled as a very viscous fluid with viscosity μ_0. Beyond a threshold in stress τ_0 the viscosity is described by a power law.

2.3. *Model validation and calibration*

In this study, we employ the VOF solver implemented in the open-source software OpenFOAM [21] to simulate laboratory-scale dam-break experiment conducted by Tang et al. [10]. The dimensions of experimental setup are adopted directly in the simulation. The model parameters are based on experimental data [10] and are specified as follows: fluid density $\rho = 1600$ kg/m^3, yield stress $\tau_0 = 5.01$ Pa, flow index $n = 0.37$ and consistency index $k = 2.04$ Pa.s$^{0.37}$. A schematic drawing of experiments flume scale test and numerical setup software are presented in Fig. 2. In this experiment, the gate was lifted to release the mud column, which subsequently flowed along the flume. The pressure was measured at several locations ($x = 1.5$ m and $x = 2.5$ m) using sensors installed on the flume bed. These measurements were compared with the results of numerical simulation to validate the model calibration (Fig. 3). Similar comparisons were also reported in [11].

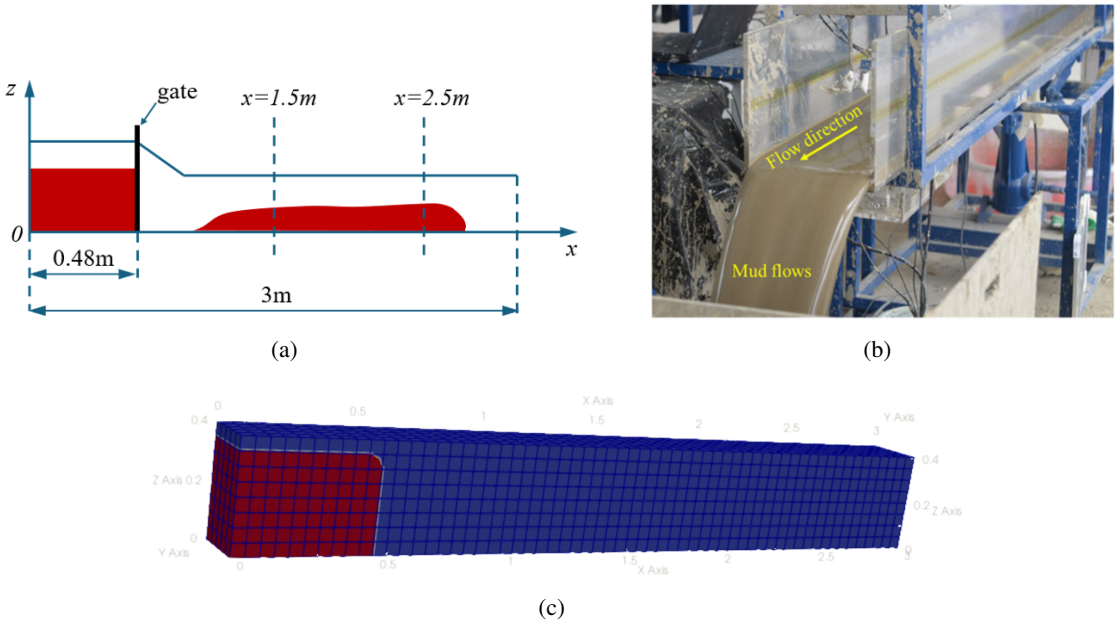

Figure 2. Experiment and numerical setups: (a,b) experiment configuration adapted from Tang et al. [10]; (c) numerical model by OpenFOAM (showing initial stage and the propagation of mudflow)

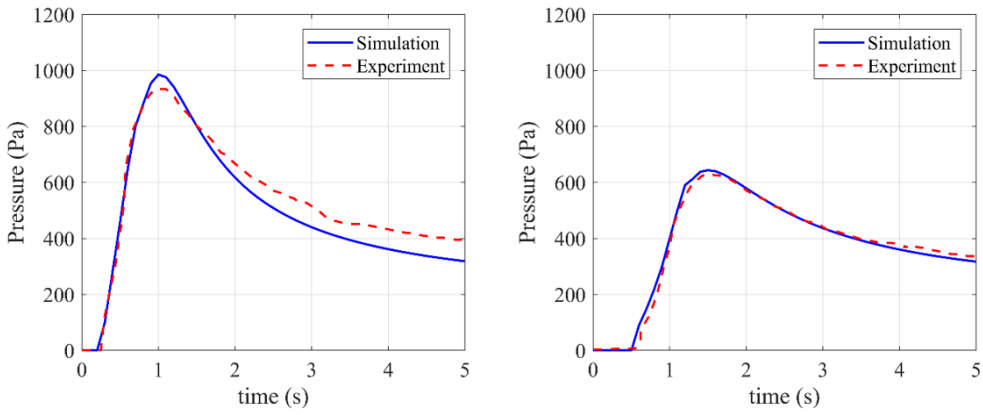

Figure 3. Comparison of pressures at flume bed between experiment and simulation

As typically observed in Herschel–Bulkley flows, the velocity profile naturally partitions into a basal shear layer and an overlying plug layer [10]. The shear zone is responsible for most of the energy dissipation, while the plug region undergoes near-rigid-body motion with minimal internal deformation. This stratification is especially pronounced on inclined planes, where gravity enhances the mobilization of the shear layer, amplifying viscous-plastic dissipation and yielding behavior.

The computed velocity profile from the VOF simulation using OpenFOAM on a horizontal bed (Fig. 4) clearly reveals the classical two-layer structure of Herschel–Bulkley flows: a basal shear layer and an overlying plug layer. In the shear layer, the velocity increases approximately linearly with height, indicating that the local shear stress exceeds the yield threshold τ_0, thereby activating plastic flow. Above this region, the velocity reaches a nearly uniform plateau, signifying a plug zone where the shear rate effectively vanishes and the fluid moves like a rigid body.

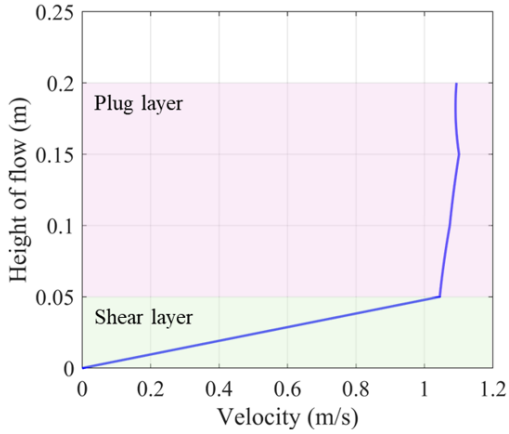

Figure 4. Typical velocity profile of the muddy flow

The simulated velocity profile exhibits a characteristic plug–shear structure, consisting of a basal shear layer and an overlying plug region, which is qualitatively consistent with analytical solutions of Herschel–Bulkley flows reported in the literature (e.g., [10]). Even in the absence of a slope, the internal stress distribution induced by gravitational loading is sufficient to develop a clear shear–plug interface. The plug occupies a large portion of the flow depth, consistent with high yield-stress and low-shear regimes commonly observed in muddy or debris flows.

3. Investigation of mudflow impact on rigid barriers

3.1. Numerical model setup

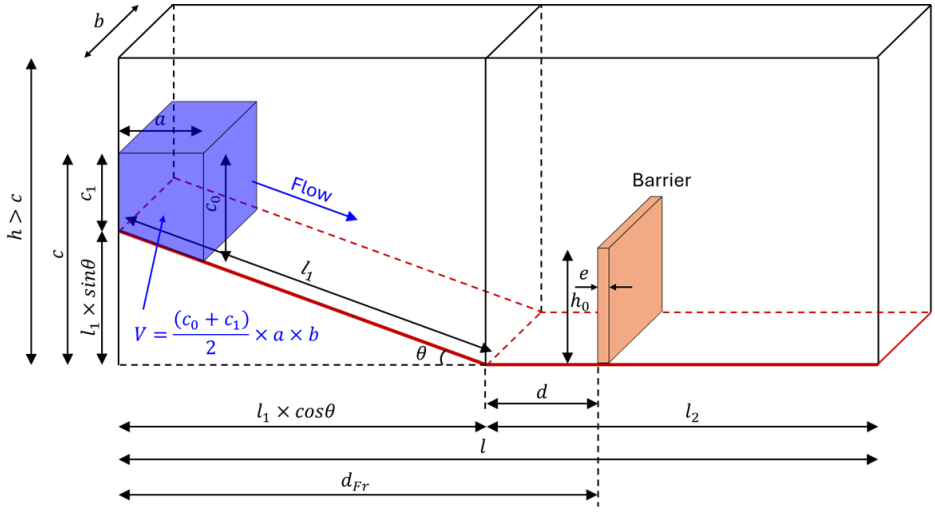

Figure 5. Conceptual model setup

To investigate the impact dynamics of the flow, a conceptual model is presented in Fig. 5. The channel consists of two parts, horizontal and inclined (or sloped) parts. The initial deposition of fluid

column is stored on the top of the channel (inclined part) when the rigid barrier is installed in the downstream (i.e. horizontal part). The fluid model parameters are taken to be the same as those given in Section 2.3. The gate was removed, and the fluid flowed down and hit the downstream barrier. In Fig. 5, the width of flume equals to $b = 0.23$ m. The length of inclined and horizontal parts is $l_1 = 1.5$ m and $l_2 = 1$ m respectively. The inclination angle (θ) and distance to the barrier (d) are varied while the height of the barrier is taken as $h_0 = 0.5$ m. In total 12 simulations are performed with detailed geometries and dimensions as given in Table 1. The fluid column dimensions are controlled by a, b, c_0 and c_1. While $a = 0.5$ m and $b = 0.23$ m for all simulations, the values of c_0 and c_1 are varied depending on the slope θ in order to obtain similar volume (V) of fluid which is approximately equal to $V = 0.035$ m^3.

Table 1. Simulation cases

Case	θ (degrees)	d (m)
B-0-25		0.25
B-0-50	0 (horizontal case)	0.50
B-0-75		0.75
B-5-25		0.25
B-5-50	5	0.50
B-5-75		0.75
B-10-25		0.25
B-10-50	10	0.50
B-10-75		0.75
B-15-25		0.25
B-15-50	15	0.50
B-15-75		0.75

3.2. Energy evolution and runup height

We now investigate the evolution of potential, kinetic and dissipated energy of the flows. These quantities are calculated during the simulation using the following equations [11, 26]:

$$E_k = \frac{1}{2} \sum_i \left(\rho \left| U_i \right|^2 \alpha_i V_i \right) \tag{7}$$

$$E_p = \sum_i \left(-\rho \left(g \cdot C_i \right) \alpha_i V_i \right) \tag{8}$$

$$E_d = E_0 - \left(E_k + E_p \right) \tag{9}$$

where E_p, E_k and E_d are respectively potential, kinetic and dissipated energy. ρ is the fluid density, α_i, U_i, V_i and C_i are fluid volume fraction, velocity, volume of cell and centroid position vector of i. E_0 is the initial potential energy.

Fig. 6 illustrates the time evolution of normalized kinetic energy E_k/E_0 and normalized dissipated energy E_d/E_0 by the initial gravitational potential energy E_0 for all inclination angles $\theta = 0^\circ, 5^\circ, 10^\circ, 15^\circ$. Note that, although the initial fluid volumes are nearly identical for all simulations, the initial potential energy varies with the angle θ. For this reason, all normalized quantities shown in this figure are computed using the case specific $E_0(\theta)$. The evolution of potential, kinetic, and

dissipated energies exhibits a strong dependence on slope inclination (θ). With increasing θ, the gravitational acceleration component along the slope ($g \sin\theta$) becomes more dominant, resulting in a faster conversion of potential to kinetic energy [10, 13, 27, 28]. Similar correlations between slope angle and energy conversion efficiency have also been reported in laboratory flume tests of non-Newtonian flows, where higher inclinations produced sharper kinetic energy peaks and higher front velocities before impact [15, 19]. At the same time, energy dissipation increases with θ due to enhanced internal shear and viscosity effects.

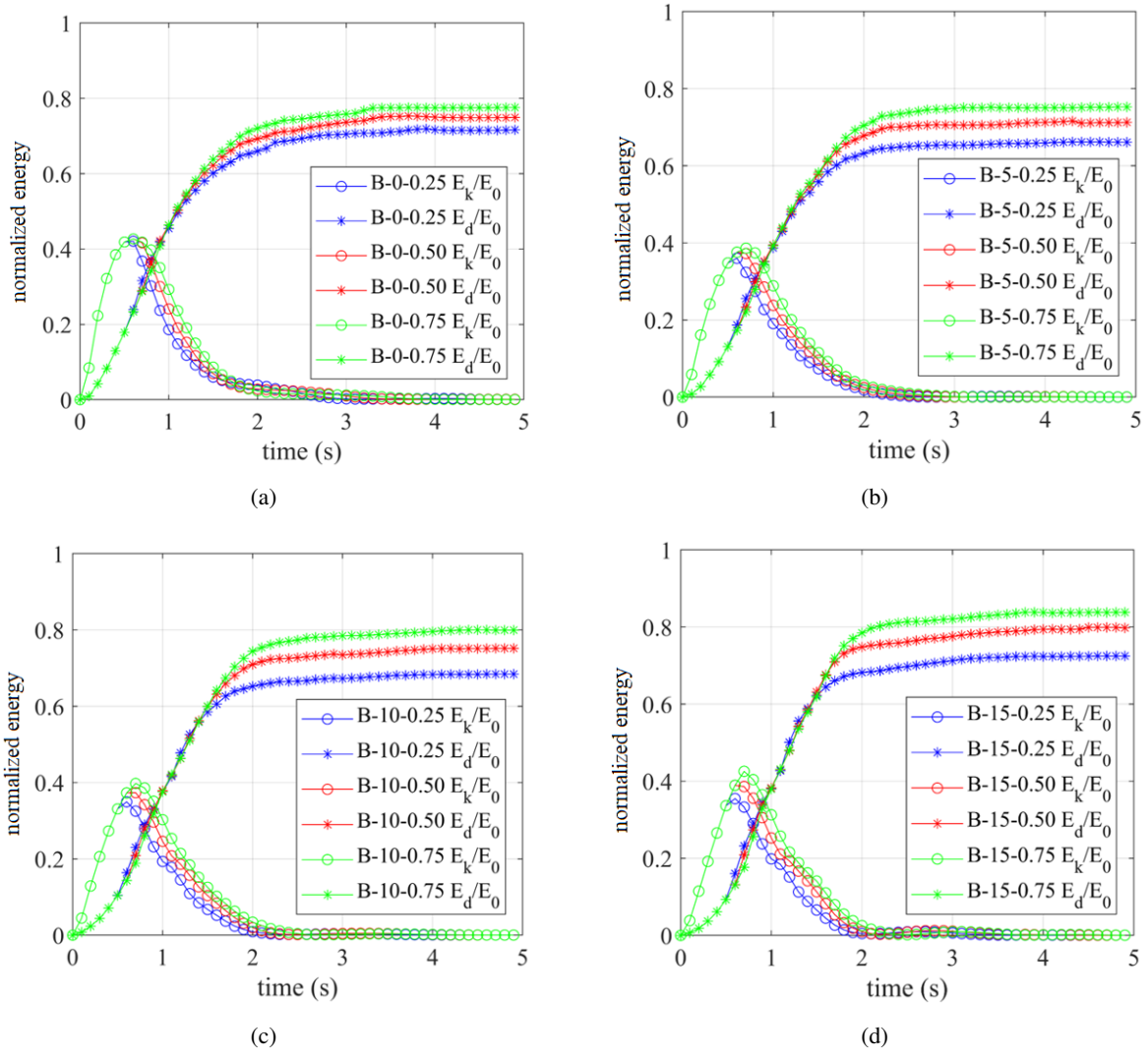

Figure 6. Normalized energy evolution: In each sub-figure, the legend is grouped by the distance d (0.25, 0.50, and 0.75 m), with E_k/E_0 and E_d/E_0 listed consecutively within each group

For a given θ (except $\theta = 0^\circ$), increasing the runout distance d (before impacting the barrier) systematically increases the fraction of initial potential energy converted into kinetic energy prior to impact. In this case, the longer travel distance permits higher pre-impact flow front velocities resulting in larger peaks E_k/E_0. For a given slope angle, increasing the barrier distance d (from the toe of the slope) results in a higher normalized kinetic energy throughout simulation. This indicates

that the flow continues to accelerate or maintain momentum over the longer runout section, despite viscous resistance. Although a larger d increases the kinetic energy of the moving mass, it does not necessarily lead to a proportionally higher impact pressure, since the flow front becomes thinner and spreads laterally, reducing local dynamic pressure on the barrier [16, 29, 30]. This behavior differs with Newtonian fluid and highlights the delayed energy release and momentum persistence typical of viscoplastic mud flows.

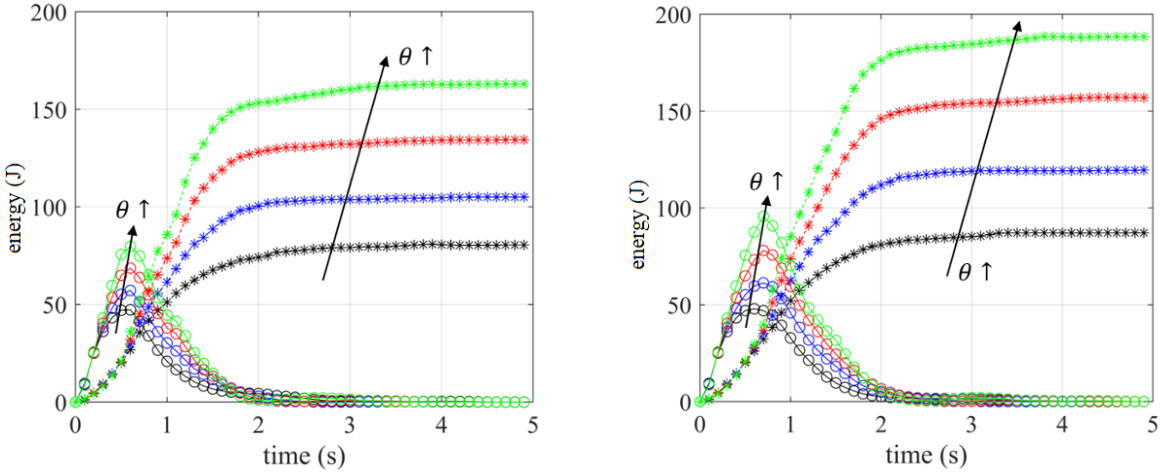

Figure 7. Effects of inclination angle on energy evolution

Increasing the slope θ of the inclined part led to: (i) altering the initial energy E_0 through a change in the center of fluid column, and (ii) increasing the component of gravitational acceleration along the flow, thus accelerating the collapse. As a consequence, comparison across θ require not only the normalized kinetic/dissipated energy by E_0 but also the absolute energy as shown in Fig. 7. Two examples of runout distance $d = 0.25$ m and $d = 0.75$ m are shown but we also found that the case with $d = 0.5$ m revealed the same observation. For all cases, both E_k and E_d show a clear increasing trend with θ, indicating that steeper slopes induce higher energy released and therefore stronger impact dynamics. This is expected since the increase in θ directly raises the initial potential energy of the fluid column, leading to greater conversion into kinetic energy during the flow. For each barrier location (d), E_k reaches a sharp peak shortly before impact followed by a rapid decrease as energy is dissipated through impact and flow fragmentation due to spreading effect. The magnitude of E_k and its peak is consistently higher for larger θ confirming the enhanced mobility and velocity of the flow front. The rate of energy dissipation also increases with θ reflecting greater fluid-barrier interaction. When comparing between different d, it is also observed that larger d allows the flow more space to accelerate prior to impact, resulting in slightly higher E_k and E_d. However, the overall difference is moderate, suggesting that the change in initial potential energy plays a more dominant role than the possible runout distance in governing energy conversion.

Fig. 8 provides a visual comparison of the flow-barrier interaction for horizontal and inclined slope conditions. In the case of $\theta = 0^\circ$ (top), the flow exhibits a relatively thin and uniform front, with limited vertical momentum upon impact. The runup height reaches approximately 0.34 m, consistent with the moderate kinetic energy observed. At $\theta = 15^\circ$ (bottom), the downslope gravitational acceleration significantly intensifies the front velocity and thickens the basal shear layer. The flow impacts on

the barrier with higher momentum, producing a more pronounced upward surge and a runup height of about 0.52 m. This visual evidence supports the energy-based interpretation discussed earlier: steeper slopes enhance the conversion of potential to kinetic energy, leading to higher runup.

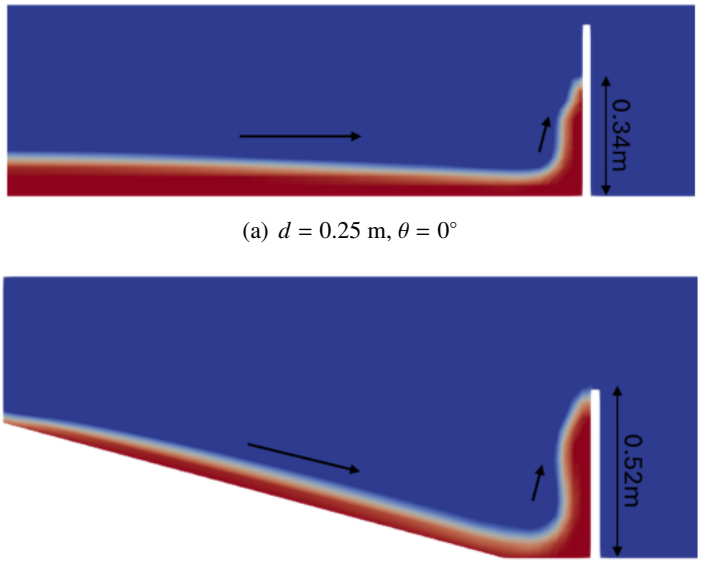

(a) d = 0.25 m, θ = 0°

(b) d = 0.25 m, θ = 15°

Figure 8. Example of runup flows for: θ = 0° (top) and θ = 15° (bottom)

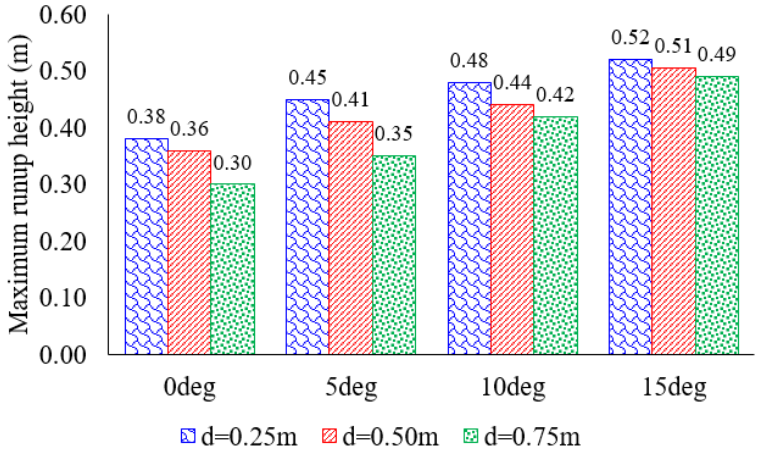

Figure 9. Variation of maximum runup height with slope inclination and barrier distance

Fig. 9 presents the variation of maximum runup height on the barrier under different slope angles (θ) and distance between the slope toe and barrier (d). Two major tendencies can be observed: (i) runup height increases consistently with slope inclination and (ii) for a given slope angle, runup height decreases with increasing barrier distance, although this effect becomes less pronounced at steeper slopes. These tendencies reflect the balance between energy production on the slope and energy dissipation during horizontal propagation. As θ increases, the downslope component of gravity ($g \sin\theta$) enhances the conversion of potential energy into kinetic energy. In the early phase on the slope, the increase of kinetic energy (E_k) is dominant, meaning that a larger fraction of the initial potential energy (E_0) is effectively transformed into useful motion. The flow thus reaches the barrier

with greater momentum, resulting in higher runup heights, increasing from 0.38 m at $\theta = 0^\circ$ to 0.52 m at $\theta = 15^\circ$ for $d = 0.25$ m. In contrast, increasing d prolongs the horizontal travel where no additional energy is gained, while friction and viscosity induce greater energy losses. Consequently, the impact energy and runup height decrease. This behavior corresponds well with both laboratory observations and numerical predictions of mud/debris flow surges impacting rigid barrier [15, 16]. Regarding engineering implication, steeper slopes yield more energetic and hazardous impact, requiring stronger or more dissipative barriers. Meanwhile, placing barriers farther from the slope toe allows more natural energy attenuation, reducing runup height structural load. However, this should be carefully reconsidered, as will be discussed in the next section when impact loads on the barriers are analyzed.

3.3. Impact dynamics

Regarding the effect of distance d, at a given slope, decreasing d (i.e., placing the barrier closer to the toe of the slope) consistently increases the peak impact force. When $d = 0.25$ m, the fluid front is still compact and maintains higher momentum upon impact, producing largest force amplitude. As d increases to 0.50 m and 0.75 m, the flow front experiences energy loss due to viscous dissipation before reaching the barrier, resulting in reduced impact magnitudes. This behavior aligns well with the earlier observation that E_d rises over time and with distance, indicating stronger energy dissipation during propagation. At later times ($t > 2$ s), secondary peaks appear, especially for steeper slopes and shorter distances. These are associated with the reflected and recirculating waves generated after the initial impact, which intermittently strike the barrier again. The persistence and amplitude of these secondary forces become more evident as θ increases, emphasizing that steeper slopes promote more energetic and oscillatory flow-structure interactions.

At steepest slope ($\theta = 15^\circ$), the peak impact force for $d = 0.25$ m and $d = 0.50$ m are observed to be nearly equal. This behavior results from the competition between two opposing effects that roughly balance each other at this slope. When barrier is positioned closer to the release point ($d = 0.25$ m), the front remains more compact and the impacting mass is more concentrated, leading to a strong but short-lived force pulse. In contrast, increasing the runout distance to $d = 0.50$ m allows the flow to accelerate over a longer path, resulting in a higher impact velocity. However, the flow front becomes more dispersed, which reduces the local pressure intensity on the barrier. At $\theta = 15^\circ$, the additional acceleration nearly compensates for the reduced mass concentration, so that the product of impact mass and squared velocity (i.e, the effective momentum flux) is comparable between the two cases. This trade-off explains both scenarios yield similar peak forces despite different runout distances. The magnitude of impact force increases substantially with θ, which agrees with both empirical relationships and numerical predictions of impact pressure scaling with Froude number [1, 4].

From an engineering perspective, this result indicates that at a steep slope, increasing the barrier setback distance (i.e., placing it further downslope), does not necessarily reduce the maximum impact load, since the higher velocity can counteract the geometric attenuation due to spreading. In practice, this suggests that barrier design for steep channels should not rely solely on distance-based mitigation (e.g., assuming that further placement always decreases impact). Instead, it is necessary to consider both slope-induced acceleration and the expected front dilution when estimating design impact forces. Conversely, for gentler slopes, the spreading effect tends to dominate, making the barrier position more effective in reducing impact. Therefore, the sensitivity of peak force to slope angle should be explicitly incorporated into design guidelines, especially for energy-dissipating or deflecting structure where kinetic-to-dissipated energy conversion strongly depends on the slope angle θ.

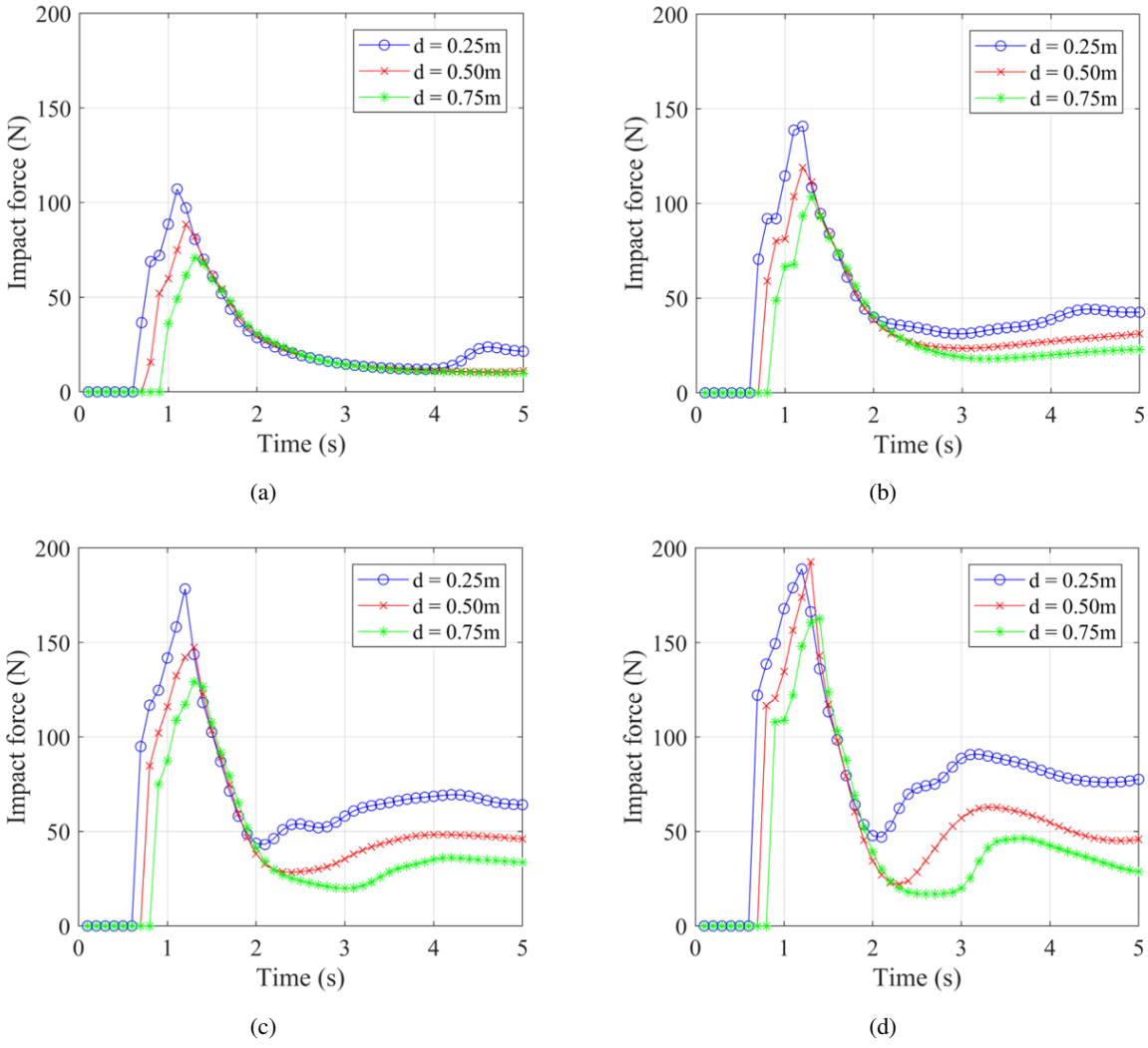

Figure 10. Impact force on barriers

4. Conclusions

This study numerically investigated the dynamics of mud and debris flow impact on rigid barriers using the VOF method with Herschel–Bulkley rheological model. The following conclusions can be drawn:

- Model validation demonstrated good agreement between simulation and experimental data, confirming the ability of the model to reproduce realistic characteristics of mudflows.

- Energy conversion strongly depends on slope inclination. Increasing the slope angle enhances the gravitational component of acceleration, leading to higher kinetic energy before impact and more intense energy dissipation during flow-barrier interaction. The increase in kinetic energy is larger than the rise in dissipation, resulting in more energetic impacts.

- Runup height rises with slope angle but decreases with barrier distance. While higher slopes amplify flow velocity and momentum, longer propagation path over a horizontal plane increases viscosity, reducing impact energy.

- Impact force dynamics show that smaller barrier distances yield higher peak force due to con-

centrated flow fronts. For steep slopes ($\theta = 15^{\circ}$), the peak forces for $d = 0.25$ m and 0.50 m become comparable, indicating a balance between increased impact velocity and reduced front concentration.

Regarding engineering implications, steeper slopes require more robust or energy-dissipating barriers due to higher kinetic and impact energies. Increasing barrier distance can effectively attenuate impact loads on gentle slopes but at high inclinations, velocity gain may reduce this effect. Thus, barrier placement and design should explicitly consider slope-dependent energy conversion and dissipation mechanisms. As consequence, this research advances the understanding of non-Newtonian flow-structure interactions and thus provides quantitative insight for optimizing the placement and structural resistance of barriers subject to mud/debris flow hazards. Building on these engineering implications, although the present study is conducted at the flume scale, the proposed CFD–Herschel–Bulkley framework can be extended to debris-flow-prone mountainous provinces (e.g. Lao Cai, Quang Nam provinces in Vietnam) by preserving similar Froude-number regimes while incorporating site-specific topography and rheological parameters derived from local materials.

Acknowledgment

This research is funded by Vietnam National Foundation for Science and Technology Development (NAFOSTED) under grant number 107.03-2023.36

References

[1] Iverson, R. M. (1997). The physics of debris flows. *Reviews of Geophysics*, 35(3):245–296.
[2] Coussot, P. (2017). *Mudflow rheology and dynamics*. Routledge.
[3] Hungr, O. (2005). Classification and terminology. 9–23.
[4] Rickenmann, D. (1999). Empirical relationships for debris flows. *Natural Hazards*, 19(1):47–77.
[5] Kien, N. T., Hieu, N. T., Nghia, H. T. (2019). A study on the ability to apply steel open-type dams against debris flow in the northern mountainous areas of Vietnam. *Journal of Science and Technology in Civil Engineering*, 13(5V):28–37. (in Vietnamese).
[6] Son, N. T., Luc, V. V., Hung, D. D., Nga, P. T., Lan, H. P., Nguyen, D. V. (2025). Experimental investigation of debris flow impact dynamics on a single rigid barrier. *Journal of Science and Technology in Civil Engineering*, 19(2V):42–57. (in Vietnamese).
[7] Major, J. J., Iverson, R. M. (1999). Debris-flow deposition: Effects of pore-fluid pressure and friction concentrated at flow margins. *Geological Society of America Bulletin*, 111(10):1424–1434.
[8] Takahashi, T. (2007). *Debris flow: Mechanics, prediction and countermeasures*. Taylor & Francis.
[9] Dai, Z., Huang, Y., Cheng, H., Xu, Q. (2016). SPH model for fluid–structure interaction and its application to debris flow impact estimation. *Landslides*, 14(3):917–928.
[10] Tang, J., Lin, P., Cui, P. (2022). Depth-resolved numerical model of dam break mud flows with Herschel-Bulkley rheology. *Journal of Mountain Science*, 19(4):1001–1017.
[11] Nguyen, T.-K., Nguyen, N. H. T., Vo, T.-T., Chen, L. (2025). Dissipative effects of baffles on the dynamics of debris flow and its impact on downstream structure. *Computers and Geotechnics*, 184:107246.
[12] Huang, X., Garcia, M. H. (1998). A Herschel–Bulkley model for mud flow down a slope. *Journal of Fluid Mechanics*, 374:305–333.
[13] Lapillonne, S., Fourtakas, G., Richefeu, V., Piton, G., Chambon, G. (2025). Towards viscous debris flow simulation using DualSPHysics v5.2: Internal behaviour of viscous flows and mixtures. *Geoscientific Model Development*, 18(19):7059–7075.
[14] Kim, B.-J., Kim, D., Yune, C.-Y. (2022). Experimental study on the impact dynamics of cylindrical baffles with a rigid barrier against debris flows. *Applied Sciences*, 12(17):8632.
[15] Ng, C. W. W., Bhatta, A., Choi, C. E., Poudyal, S., Liu, H., Cheung, R. W. M., Kwan, J. S. H. (2024). Effects of debris flow rheology on overflow and impact dynamics against dual-rigid barriers. *Géotechnique*, 74(12):1172–1185.
[16] Scheidl, C., Friedl, C., Reider, L., Wernhart, S., Fuchs, A.-L., Dankwerth, A. L., Nagl, G., Kaitna, R., Proske, D. (2023). Impact dynamics of granular debris flows based on a small-scale physical model. *Acta Geotechnica*, 19(6):3979–3997.

[17] Liu, D., You, Y., Liu, J., Li, Y., Zhang, G., Wang, D. (2019). Spatial-temporal distribution of debris flow impact pressure on rigid barrier. *Journal of Mountain Science*, 16(4):793–805.
[18] Liu, X., Ma, J., Tang, H., Zhang, S., Huang, L., Zhang, J. (2020). A novel dynamic impact pressure model of debris flows and its application on reliability analysis of the rock mass surrounding tunnels. *Engineering Geology*, 273:105694.
[19] Muñoz, F., Vega, J., Hidalgo, C. (2025). Experimental and numerical mudflows modeling for runout and deposition height assessment. *Natural Hazards*, 121(20):23723–23754.
[20] Lomax, H., Pulliam, T. H., Zingg, D. W. (2001). *Fundamentals of computational fluid dynamics*. Springer.
[21] Jasak, H., Jemcov, A., Tukovic, Z. (2007). OpenFOAM: A C++ library for complex physics simulations. 1–20.
[22] Gamet, L., Scala, M., Roenby, J., Scheufler, H., Pierson, J.-L. (2020). Validation of volume-of-fluid OpenFOAM® isoAdvector solvers using single bubble benchmarks. *Computers and Fluids*, 213:104722.
[23] Færgestad, I. (2016). *The defining series: Rheology*.
[24] De Blasio, F. V. (2011). Non-Newtonian fluids, mudflows, and debris flows: A rheological approach. 89–130.
[25] Yin, D., Zhang, W., Cheng, C., Li, Y. (2012). Fractional time-dependent Bingham model for muddy clay. *Journal of Non-Newtonian Fluid Mechanics*, 187-188:32–35.
[26] Nguyen, N. H. T., Nguyen, T. T., Phan, Q. T. (2022). Dynamics and runout distance of saturated particle-fluid mixture flow on a horizontal plane: A coupled VOF-DEM study. *Powder Technology*, 408:117759.
[27] Bi, Y., Huang, Y., Zhang, B., Pu, J. (2024). CFD-DEM numerical investigation of the effects of water content and inclination angle on interactions between debris flows and slit dam. *Computers and Geotechnics*, 170:106273.
[28] Anh, Q. V., Manh, N. D., Thao, L. V., Trung, V. T. (2024). Energy evolution of gravitational-granular flows. *Journal of Science and Technology in Civil Engineering (JSTCE)-HUCE*, 18(1):143–152.
[29] Huo, M., Zhou, J., Zhao, J., Zhou, H., Li, J., Liu, X. (2023). The normal impact stiffness of a debris-flow flexible barrier. *Scientific Reports*, 13(1):3969.
[30] Yu, X., Li, W., Zhang, G. (2024). Research on the distribution of debris flow impact on the upstream surface of the check dam. *Scientific Reports*, 14(1):25281.